

# Dynamical evolution of non-minimally coupled scalar field in spherically symmetric de Sitter spacetimes

R. B. Fontana\*

*Universidade Federal da Fronteira Sul,  
Campus Chapecó, CEP 89802-112, SC, Brazil*

Jeferson de Oliveira†

*Instituto de Física, Universidade Federal de Mato Grosso, CEP 78060-900, Cuiabá, Brazil*

A. B. Pavan‡

*Universidade Federal de Itajubá, Instituto de  
Física e Química, CEP 37500-903, Itajubá, Brazil*

(Dated: May 11, 2019)

## Abstract

We investigate the dynamical behavior of a scalar field non-minimally coupled to Einstein's tensor and Ricci scalar in geometries of asymptotically de Sitter spacetimes. We show that the quasinormal modes remain unaffected in the chargeless case for the massless scalar field. In the massive case, the coupling of both parameters produces a region of instability in the spacetime determined both by the geometry parameters and by the wavenumber  $l$ . In the Schwarzschild case, every solution for the movement equations with  $l > 0$  has a range of values of the coupling constant that produces unstable modes. The case  $l = 0$  is the most unstable one, with a threshold value for stability in the coupling. For the charged black hole, the existence of a range of instability in  $\eta$  is strongly related to geometry parameters presenting a region of stability independent of the parameter chosen.

---

\* rodrigo.fontana@uffs.edu.br

† jeferson@gravitacao.org

‡ alanbpavan@gmail.com

## I. INTRODUCTION

The evolution of probe fields in black hole backgrounds has long been a very active field of research in theoretical physics [1–3, and references therein]. Probe field profiles in the time domain present a discrete set of complex frequencies called quasinormal frequencies (QNFs) that can provide valuable information about the structure of spacetime. Each of these frequencies corresponds to a damped vibrational mode of the field, the so-called quasinormal mode (QNM). The set of QNMs carry specific information about the signature of the geometry (e. g. black hole solutions), since it depends only on the parameters that define the metric.

The applications of quasinormal modes are manifold: probing the linear stability of black holes and stars spacetimes [40]; identification of astrophysical black holes through gravitational waves signals [3], experimentally verified by LIGO [4] [5]; studying the role played by such oscillations in the context of gauge/gravity duality, especially in the AdS/CFT [7] [8] [10] [11] [12] and dS/CFT correspondences [13, 14].

The stability of black holes and stars has been discussed in several works [15] since the 50's with the original paper of Regge and Wheeler analyzing the Schwarzschild singularity [6]. The QNM's of scalar, abelian gauge, and fermionic probe fields evolving in the neighborhood of black holes have also been used to obtain insights about the nature of spacetime. In the case of asymptotically flat black holes these QNM's are, by the no-hair theorems, functions of only the mass  $M$ , the electric charge  $Q$ , and the angular momentum  $L$  of the black hole [16]. However, more recently, these theorems were circumvented in the asymptotically AdS black holes and other configurations with non-minimally coupled fields such that hairy black holes solutions have been found [17–20, 26]. In the latter cases, the QNM's depend on other hairs of the spacetime, and black hole phase transitions are present.

In AdS/CFT correspondence context, a robust interpretation for the QNM spectra in the view of a quantum field theory at finite temperature (defined at the AdS boundary) is provided: the inverse of the imaginary part of the fundamental quasinormal frequency is understood as a relaxation time of the dual operator at the border [8]. Among the applications of AdS/CFT correspondence to condensed matter physics [9, and references therein], we mention the phase transitions at the border theory giving rise to the so-called holographic superconductors [21–25]: the phenomena yields a specific bulk effect through the

QNMs, i.e, growing/decaying oscillations of a given probe field in the bulk correspond to a conductive/superconducting phase at the dual field theory [26]. The presence of instabilities (growing modes) in the quasinormal spectrum therefore indicates a phase transition at the border.

On the dS/CFT correspondence [31], the evolution of probe fields on the gravity side is related to fundamental quantities in the border field theory [14] [13]: the poles of the two-point correlator of the three-dimensional conformal field theory at the boundary scale perfectly the QNMs spectrum of a massive scalar field in the de Sitter spacetime.

Non-minimally coupled (NMC) curvature models were firstly considered in the late 80's [39], as an alternative gravitation theory. The presence of a scalar field coupled to curvature terms in Einstein-Hilbert action allows for a suitable solution for the inflation exit, and in general has a de Sitter spacetime as the attractor for later times, as should be expected. Besides the traditional terms of NMC models, a few years later, derivative terms were introduced in the action [37], expanding the possibilities for the scalar field potential, characterizing the NMDC models. From the possible derivative terms, only two significant contributions are in general considered. With a particular scale of the Lagrangian couplings and the cosmological constant, the inflation scenario is generated, as well as the de Sitter spacetime remnant from the curvature equations [36].

The curvature equations coming from NMDC models are of third or higher order, in general. For a particular choice of couplings, however, it is still possible to achieve second order equations: when the Lagrangian derivative terms are placed as Einstein tensor coupled to scalar field components [35]. This choice turns the NMDC into a more suitable (simple) form, as it makes it unnecessary to fine tune the scalar field potential.

Beyond the strategic elimination of the fine tuning problem, another possible purpose of the coupling is to perform as a dark matter component, feasible in the form of  $\Lambda$ CDM model [34]. The rate of the scalar field density and total density in the model is slightly different from that of a cold dark matter model, but still in the observationally allowed range. Once NMDC models could be used to describe dark energy and dark matter, they would be instrumental to understand how this coupling affects black holes: for instance, in the context of scalar-tensor gravity exact hairy black hole solutions have been found using NMDC models [18, 19].

In this work we concern ourselves with the dynamical evolution of a scalar field in different

geometries with the non-minimal derivative coupling introduced in the action as

$$S = \int d^4x \sqrt{-g} [F(\Phi, R, R_{\mu\nu}R^{\mu\nu}, R_{\mu\nu\delta\sigma}R^{\mu\nu\delta\sigma}) + H(\Phi, \partial_\sigma\Phi\partial^\sigma\Phi, \nabla^2\Phi) + V(\Phi)], \quad (1)$$

where the function  $F$  encodes all possible Lagrangian curvature terms along with their couplings to a scalar field component  $\Phi$ ,  $H$  gives a general coupling between curvature and the scalar field kinetic term, and  $V(\Phi)$  is the scalar field potential. This action is relevant, e. g., in the context of quantum gravity [32], where additional terms in the curvature of most second degree are added to the Einstein-Hilbert Lagrangian. Although the correspondent gravity theory is not unitary, it can be considered as the starting point of an effective theory of gravity, since the description of it does not have to satisfy all requirements imposed by the fundamental physics. As a particular case of action (1), we can consider the simplest NMDC model with matter terms as follows:

$$S = \int d^4x \sqrt{-g} [\mathcal{L}_{\text{background}}(\mathcal{R}, \Lambda, F^{\mu\nu}) + \mathcal{L}_{\text{perturbative}}(\Phi)], \quad (2)$$

where

$$\mathcal{L}_{\text{background}}(\mathcal{R}, \Lambda, F^{\mu\nu}) = \frac{\mathcal{R}}{16\pi G} + \frac{6}{L^2} - \frac{F_{\mu\nu}F^{\mu\nu}}{4}, \quad (3)$$

with  $\mathcal{R}$  standing for the Ricci scalar,  $L$  is the dS radius and  $F_{\mu\nu}$  are the components of electromagnetic field strength tensor. Also,

$$\mathcal{L}_{\text{perturbative}}(\Phi) = \frac{1}{2} (g^{\mu\nu} + \eta G^{\mu\nu}) \partial_\mu\Phi\partial_\nu\Phi + m^2\Phi^2 + V_{\text{int}}(\Phi), \quad (4)$$

where  $g_{\mu\nu}$  and  $G_{\mu\nu}$  are, respectively, the components of metric and Einstein tensors,  $\Phi$  is the probe scalar field with mass  $m$  and  $\eta$  is the NMC parameter. Here we are interested in the effect produced on the scalar field equation, given usual black hole geometries. Notice that the effects of the coupled scalar field on the geometry are secondary when compared with that of matter [33].

The paper is organized as follows: in section II we establish a general equation of motion for the scalar field  $\Phi$  for spherically symmetric spacetimes. In sections III-V we analyze the dynamical properties of the field the spacetimes of de Sitter, Schwarzschild-de Sitter, and Reissner-Nordström-de Sitter, respectively, being the quasi-extremal case studied in section VI. In section VII we present our conclusions and final remarks relative to peculiar features of the coupling for all geometries.

## II. EQUATION OF MOTION

We first consider the four-dimensional spherically symmetric black hole background solution, namely

$$ds^2 = -f(r) dt^2 + \frac{1}{f(r)} dr^2 + r^2 d\Omega^2, \quad (5)$$

with  $d\Omega^2 = d\theta^2 + \sin^2\theta d\phi^2$  representing the 2-sphere line element. The equation of motion for the scalar field  $\Phi$  derived from the action (2) is given by

$$\frac{1}{\sqrt{-g}} \partial_\mu \left( \sqrt{-g} h^{\mu\nu} \partial_\nu \Phi \right) - \frac{dV}{d\Phi} = 0, \quad (6)$$

where  $V$  the potential of the scalar field and

$$h^{\mu\nu} = g^{\mu\nu} + \eta G^{\mu\nu}, \quad (7)$$

acts as an induced metric for the scalar field equation, through  $\eta$ . Besides a mass term, the simplest non-minimal coupling via Ricci scalar  $\mathcal{R}$  in the potential is written as

$$V_{int}(\Phi) = \xi \mathcal{R} \Phi^2. \quad (8)$$

Applying the standard ansatz to separate variables in spherically symmetric spacetimes we write the field in radial-temporal and angular parts,

$$\Phi(t, r, \theta, \phi) = \sum_{lm} R(r, t) Y_{lm}(\theta, \phi), \quad (9)$$

which, introduced into Eq. (6), yields

$$-\frac{\partial^2 R}{\partial t^2} + \alpha \frac{\partial^2 R}{\partial r^2} + \alpha \left( \frac{2}{r} + \frac{dF}{dr} \right) \frac{\partial R}{\partial r} - V(r)R = 0, \quad (10)$$

with the effective potential  $V(r)$  being

$$V(r) = \frac{\beta \ell(\ell+1)}{r^2} + \gamma (m^2 + \xi \mathcal{R}), \quad (11)$$

and the functions  $\alpha(r)$ ,  $\beta(r)$ ,  $\gamma(r)$  and  $F(r)$  given by,

$$\alpha = \frac{(1 + \eta B)}{(-\eta A)} f(r)^2, \quad (12)$$

$$\beta = \frac{(1 + \eta C)}{(1 - \eta A)} f(r), \quad (13)$$

$$\gamma = \frac{f(r)}{(1 - \eta A)}, \quad (14)$$

$$F = \ln [(1 + \eta B) f(r)]. \quad (15)$$

Functions  $A, B$  and  $C$  are specific of each geometry and defined in the appendix. In order to place (10) as a Schrödinger equation, we perform a change in the radial coordinate to the tortoise system,  $\frac{dr_*}{dr} = \frac{1}{f} \sqrt{\frac{1-\eta A}{1+\eta B}}$  resulting in

$$-\frac{\partial^2 \tilde{R}}{\partial t^2} + \frac{\partial^2 \tilde{R}}{\partial r_*^2} + \tilde{V}(r) \tilde{R} = 0, \quad (16)$$

where  $R = \frac{\tilde{R}(r, t)}{r[(1-\eta A)(1+\eta B)]^{1/4}}$ . This new coordinate system has the advantage of avoiding singularities in the integration of the scalar field equation encapsulating it beyond the event horizon. In this case, the above effective potential is written as

$$\begin{aligned} \tilde{V}(r) = \frac{\alpha}{16} \left[ \frac{5\eta^2 A^2}{(-1+\eta A)^2} + \frac{\eta^2 B^2}{(1+\eta B)^2} - \frac{16f'}{rf} - \frac{4\eta B'(4f+rf')}{r(1+\eta B)f} \right. \\ \left. - \frac{2\eta A'(\eta f B' + 2(1+\eta B)f')}{(-1+\eta A)(1+\eta B)f} + \frac{4\eta A''}{1-\eta A} - \frac{4\eta B''}{1+\eta B} \right] - V(r), \quad (17) \end{aligned}$$

which allows us to integrate and use different methods to attain the scalar field profiles in the time domain as well as the quasinormal spectra.

### III. QNM'S FOR NON-MINIMALLY COUPLED SCALAR FIELDS EVOLVING IN THE PURE DE SITTER SPACETIME

In order to understand the evolution of non-minimal coupling scalar fields in asymptotically dS spacetimes, we firstly analyze the pure dS case, in which an analytical expression for the scalar QNMs was found in [45], where the probe scalar field is not coupled to the Einstein tensor ( $\eta = 0$  in the Lagrangian (4)).

In (3 + 1) dimensions, the line element of dS spacetime can be cast as

$$ds^2 = - \left( 1 - \frac{r^2}{L^2} \right) dt^2 + \frac{1}{(1 - r^2/L^2)} dr^2 + r^2 d\Omega^2, \quad (18)$$

where  $L$  stands for the dS radius, related to the cosmological constant  $\Lambda$  by  $L^2 = 3/\Lambda$ , and  $d\Omega^2$  is the unit 2-sphere line element. Considering the evolution of a probe scalar field with mass  $m$  in the pure dS geometry, the corresponding effective potential reads

$$V(r) = \frac{\mathcal{C}_1}{L^2 \cosh^2(r_*/L)} + \frac{\mathcal{C}_2}{L^2 \sinh^2(r_*/L)}, \quad (19)$$

with the radial tortoise coordinate  $r_* = L \operatorname{arctanh}(r/L)$ ,  $\mathcal{C}_1 = -2 + m^2 L^2$ , and  $\mathcal{C}_2 = \ell(\ell + 1)$ .

We can generalize the results for the scalar QNFs found in [45],  $\omega_{I,II}$ , considering a NMC term  $\eta \neq 0$ :

$$\omega_I = -\frac{i}{L} [2n + \ell + h_{\pm}], \quad (20)$$

$$\omega_{II} = -\frac{i}{L} [2n - (\ell + 1) + h_{\pm}], \quad (21)$$

where,

$$h_{\pm} = \frac{3}{2} \pm \sqrt{\frac{9}{4} - \frac{m^2 L^4}{L^2 - 3\eta}}. \quad (22)$$

From these exact expressions it is clear that the behavior of the coupling parameter  $\eta$  will affect the quasinormal spectrum. If  $\eta$  is bounded by  $\eta < L^2/3$ , the range of allowed values for  $m$  in order to have QNFs with non-null real part is

$$m > \frac{3}{2L} \sqrt{1 - \frac{3\eta}{L^2}}, \quad (23)$$

which constraints the field mass to be positive definite. Using the expression (22) into the Eqs (20), the two sets fo QNFs can be cast in the form

$$\omega_I = \pm \frac{1}{L} \left( \frac{m^2 L^4}{L^2 - 3\eta} - \frac{9}{4} \right)^{1/2} - \frac{i}{L} \left( 2n + \ell + \frac{3}{2} \right), \quad (24)$$

$$\omega_{II} = \pm \frac{1}{L} \left( \frac{m^2 L^4}{L^2 - 3\eta} - \frac{9}{4} \right)^{1/2} - \frac{i}{L} \left( 2n - \ell + \frac{1}{2} \right). \quad (25)$$

These expressions generalize the previous results found for the scalar field trivially coupled to the geometry [45]. In what follows, we show the existence of a region of parameters in which purely imaginary and unstable QNMs arise in the system, the origin of the instabilities attributed to the non-canonical coupling between the scalar field and the dS geometry.

### A. Purely imaginary frequencies and instabilities

Using the expressions for the frequencies found above, in this section we constraint the values of the non-canonical coupling parameter  $\eta$  and the scalar field mass  $m$  in order to get purely imaginary QNMs and, more interesting, a range of parameters allowing growing modes, i.e., frequencies with positive imaginary part.

Purely imaginary frequencies have been found in the context of black hole perturbations, and its applications to the AdS/CFT correspondence are manifold. In [27] the authors found a close relation between the Korteweg-de Vries equation and the three dimensional Lifshitz black hole in New Massive Gravity (NMG). They also showed that the scalar QNMs in the hydrodynamic limit are purely imaginary, which in the view of linear response theory corresponds to a solitonic solution. Also in the context of NMG, purely imaginary QNMs were found beyond the hydrodynamic limit in [28]. Furthermore, purely imaginary spectra have been found for a probe scalar field evolving on the geometry of  $d$ -dimensional Lifshitz black hole [29] and for the Chern-Simmons sector of  $d$ -dimensional Lovelock black holes [30].

An attempt to give an interpretation of QNMs in the framework of the dS/CFT correspondence [31] was made in [13], where the authors considered the exact QNM spectrum of scalar perturbations on a three-dimensional rotating dS black hole and in [14] for a pure  $d$ -dimensional dS black hole. In [13], it was found an exact relation between the QNM spectrum and the spectrum of thermal excitations of a Conformal Field Theory, which presents growing modes, leading to regions of instability. Following the same procedure as in [13], it is possible to show that there are growing modes and regions of instability in the case of the 4-dimensional dS spacetime with  $\eta \neq 0$ .

If we take  $L = 1$  and  $\ell = 0$  in the first set of QNMs  $\omega_I$  (24), the condition to obtain purely imaginary QNFs is that  $\eta > 1/3$ , thus

$$\omega_I = i \left[ \pm \left( \frac{m^2}{3\eta - 1} + \frac{9}{4} \right)^{1/2} - \left( 2n + \frac{3}{2} \right) \right]. \quad (26)$$

Considering then the fundamental mode  $n = 0$  for the positive branch of  $\omega_I$  and setting for simplicity  $\eta = 2/3$ , we find that the fundamental QNF corresponds to a purely growing mode for  $m^2 > 0$ . For  $\eta \rightarrow \infty$ , the QNFs of the positive branch is bounded by  $\omega_I^+ = -2ni$ , while in the negative branch  $\omega_I^-$  we have only decaying QNFs for positive masses, bounded by  $\omega_I^- = -(3 + 2n)i$ .

The same analysis can be done for the second set of QNFs (25), leading to

$$\omega_{II} = i \left[ \pm \left( \frac{m^2}{3\eta - 1} + \frac{9}{4} \right)^{1/2} - \left( 2n + \frac{1}{2} \right) \right]. \quad (27)$$

For the positive branch, the fundamental QNF is a growing mode for  $m^2 > 0$  (setting  $\eta > 2/3$ ) and for the negative branch there is only QNFs with negative imaginary part. When  $\eta \rightarrow \infty$ , these frequencies are bounded by  $\omega_{II}^- = -(2n + 2)i$  and  $\omega_{II}^+ = -(2n - 1)i$ .



In short, growing purely imaginary QNMs in the positive branch of the two sets of exact frequencies are present in the spectra, featuring two regions of instability. In Table I the fundamental frequencies are shown for several values of the coupling constant  $\eta$ .

The result for the poles of the two-point correlator function in 4- dimensional dS spacetime found in [14] can be easily generalized for the case of a non-vanishing parameter  $\eta$  by means of the following rescaling of the scalar field mass,

$$m^2 \rightarrow \frac{m^2 L^2}{L^2 - 3\eta}, \quad (28)$$

in which case the poles are written as

$$\omega = \pm \frac{i}{L} (h_{\pm} + l + 2n), \quad (29)$$

where  $h_{\pm}$  is given in (22). The above expression is equivalent to the first set of QNMs (20), therefore, the positive branch of the poles coincides with the region of instability discussed in the preceding analysis. Such a result seems to be in agreement with the dS/CFT correspondence, namely, the regions of instability in the bulk QNM spectrum matches with those obtained by the calculation of Hadamard two-point function.

TABLE I. Fundamental quasinormal modes for non-minimally coupled scalar field evolving in a pure de-Sitter spacetime for different values of  $\eta$  with  $m = 1$ ,  $L = 1$  and  $l = 0$

| $\eta$   | $\omega_I^+$ | $\omega_I^-$ | $\omega_{II}^+$ | $\omega_{II}^-$ |
|----------|--------------|--------------|-----------------|-----------------|
| 1/3      | $\infty$     | $-\infty$    | $\infty$        | $-\infty$       |
| 2/3      | $0.30277i$   | $-3.30278i$  | $1.30278i$      | $-2.30278i$     |
| 1        | $0.15831i$   | $-3.15831i$  | $1.15831i$      | $-2.15831i$     |
| 4/3      | $0.10727i$   | $-3.10728i$  | $1.10728i$      | $-2.10728i$     |
| 5/3      | $0.08114i$   | $-3.08114i$  | $1.08114i$      | $-2.08114i$     |
| 2        | $0.06525i$   | $-3.06525i$  | $1.06525i$      | $-2.06525i$     |
| 7/3      | $0.05456i$   | $-3.05456i$  | $1.05456i$      | $-2.05456i$     |
| 8/3      | $0.04689i$   | $-3.04689i$  | $1.04689i$      | $-2.04689i$     |
| 10       | $0.01145i$   | $-3.01145i$  | $1.01145i$      | $-2.01145i$     |
| $\infty$ | $0.0i$       | $-3.0i$      | $1.0i$          | $-2.0i$         |

#### IV. QNM'S FOR NON-MINIMALLY COUPLED SCALAR FIELD EVOLVING IN SCHWARZSCHILD-DE SITTER SPACETIME

The coupled-scalar field equation introduced in section II, can also be studied in a Schwarzschild-de Sitter geometry (SdS), being  $f(r) = 1 - (2M/r) - (r^2/L^2)$  the  $g_{tt}$  element of the metric.

Substituting the metric and the Einstein tensor components into Eq. (6) and using

$$\alpha = f^2, \quad \beta = f, \quad \gamma = \frac{f}{\left(1 - \frac{3\eta}{L^2}\right)}, \quad F = \ln \left[ \left(1 + \frac{3\eta}{L^2}\right) f \right], \quad (30)$$

we obtain the equation of motion for the scalar field:

$$-\frac{\partial^2 R}{\partial t^2} + f^2 \frac{\partial^2 R}{\partial r^2} + \left( \frac{2f^2}{r} + ff' \right) \frac{\partial R}{\partial r} - V(r)R = 0, \quad (31)$$

with the effective potential

$$V(r) = f(r) \left[ \frac{\ell(\ell+1)}{r^2} + \frac{\mu^2 L^2 + 12\xi}{L^2 - 3\eta} \right]. \quad (32)$$

Rewriting Eq. (31) in terms of the tortoise coordinate  $r_*$  introduced above and making the following substitution for the field,

$$R(t, r) = \frac{\tilde{R}(r, t)}{r} \quad (33)$$

we have the typical wave equation in a simple form

$$-\frac{\partial^2 \tilde{R}}{\partial t^2} + \frac{\partial^2 \tilde{R}}{\partial r_*^2} - \tilde{V}(r)\tilde{R} = 0, \quad (34)$$

with the effective potential given as

$$\tilde{V}(r) = \left( 1 - \frac{2M}{r} - \frac{r^2}{L^2} \right) \left[ \frac{\ell(\ell+1)}{r^2} + \frac{m^2 L^2}{L^2 - 3\eta} + \frac{2M}{r^3} - \frac{2}{L^2} \right]. \quad (35)$$

Here the  $m^2$  term was rescaled as the effective mass of the scalar field, being a function of the ordinary mass  $\mu$  and of the Ricci-coupling introduced in the perturbed potential:  $m^2 = (\mu^2 + 12\xi/L^2)$ . This term is essential in the Schwarzschild case, since without which there would be no influence coming from the induced metric term  $\eta$  on the equation of motion for the scalar field. A different situation is seen in the Reissner-Nordstroem.

### A. Effective Potential

There are four qualitative different cases for the effective potential, assuming  $m \neq 0$ , depending on the metric parameters and coupling. For  $m = 0$ , in the Schwarzschild-de Sitter geometry without coupling, we will have also negative regions in the potential when  $l = 0$ , which however does not indicate the presence of unstable modes in the geometry [52]: in general, the field evolves to a constant value scaled with the cosmological constant. In this section we investigate the cases with non-zero coupling in the scalar field potential.

We denote the region between horizons as  $\mathbb{X}$  and the corresponding potential,  $V_{\mathbb{X}}$ , restraining the evolution of the scalar field to this region.

The four different regions for the potential depend on the scope of  $\eta$ . For the particular case of  $M = \ell = m = L/6 = 1$ , the signal of the potential as a function of  $\eta$  is summarized in table IV A.

| Case  | $\eta$ -range                    | Sign of $V_{\mathbb{X}}$                      |
|-------|----------------------------------|---|
| (i)   | $\eta < L^2/3$                   | $V_{\mathbb{X}} > 0$                          |
| (ii)  | $L^2/3 < \eta < \eta^{(1)}$      | $V_{\mathbb{X}} < 0$                          |
| (iii) | $\eta^{(1)} < \eta < \eta^{(2)}$ | $V_{\mathbb{X}} < 0$ and $V_{\mathbb{X}} > 0$ |
| (iv)  | $\eta > \eta^{(2)}$              | $V_{\mathbb{X}} > 0$                          |

TABLE II. The qualitatively different regions of the effective potential for  $M = \ell = m = L/6 = 1$ .

Here the specific values of  $\eta$  in the table are given by

$$\eta^{(1)} = \frac{L^2}{3} \left[ \frac{m^2 + \frac{2M}{r_h^3} + \frac{l(l+1)}{r_h^2} - \frac{2}{L^2}}{\frac{2M}{r_h^3} + \frac{l(l+1)}{r_h^2} - \frac{2}{L^2}} \right] \simeq 38.61, \quad \eta^{(2)} = \frac{L^2}{3} \left[ \frac{m^2 + \frac{2M}{r_c^3} + \frac{l(l+1)}{r_c^2} - \frac{2}{L^2}}{\frac{2M}{r_c^3} + \frac{l(l+1)}{r_c^2} - \frac{2}{L^2}} \right] \simeq 188.64, \quad (36)$$

with  $r_h$  the event horizon and  $r_c$  the cosmological one.

The table with the potential signs is the same for any value of  $l \neq 0$ . In this case, we may have only regions (i) to (iii). Only unstable modes exist in regions (ii) and (iii) when  $l = 0$  as shown in the next section.

The Schwarzschild-de Sitter solution admits cases (i) and (iii) (for  $l = 0$ ) for which the scalar field evolves in time to a constant value or as quasinormal ringing. The  $\eta$ -coupling introduces a region of negative potential (with only unstable modes being found in this region) in addition to unstable modes when the potential alternates [seria “oscillates”?] in (iii) (an absent behavior in the  $\eta \rightarrow 0$  limit).

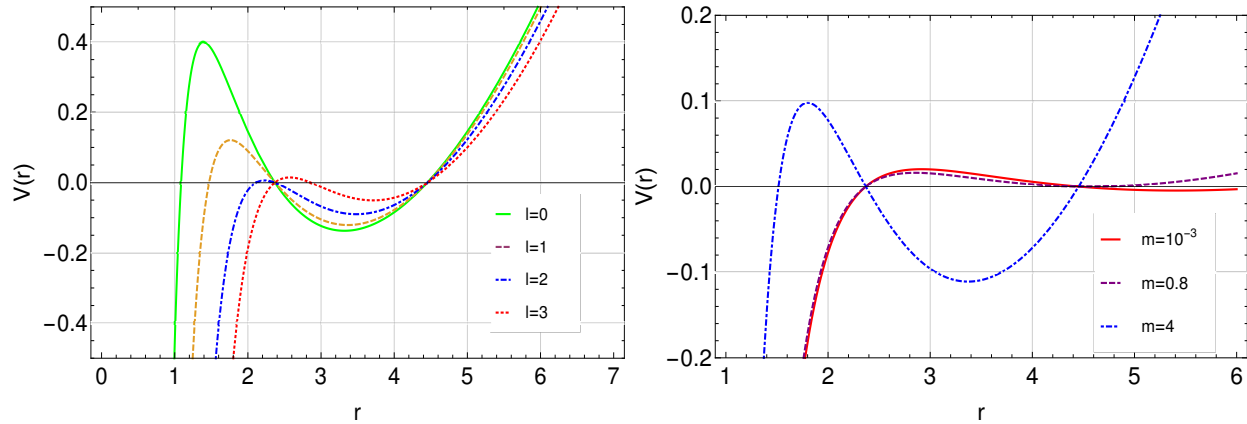


FIG. 1. Effective potential with parameters  $M = L/6 = 1$ . The horizons lie at  $r_h = 2.37$  and  $r_c = 4.45$ . Left panel: different values of  $l$  and  $\eta = 20m = 20$ . Right panel: different values of  $m$  and  $\eta = 75l = 150$ .

As we see in figure 1, the potential strongly varies its qualitative behavior as we change the scalar field mass or the multipole number  $l$ , going from regions of only stable modes to the ones in which unstable modes can be seen. This is related to the specific values of  $\eta$  showed in equations (36) above. The transition from stable to unstable modes caused by the change of  $\eta$  is expected to be related to a second order phase transition in the CFT side of the AdS/CFT correspondence [38].

Bellow, we analyze the dynamics of scalar fields subjected to these potentials, collecting the quasi-normal resonances.

## B. Scalar Field Dynamics and QNM's

The general behavior of the scalar field evolution is that of a damped oscillator. It exhibits however, a different behavior when the potential is not entirely positive between horizons. In this case unstable modes can emerge and the geometry is then expected to change. Different

evolutions (qualitatively), such as exponential decay or convergence to a constant value can also emerge - in which case the spacetime is supposed to be stable against small scalar field perturbations. All cases arise for  $L^2 > 27M^2$ , which is the causal structure condition for the presence of an encapsulated singularity (by the event horizon) and a cosmological horizon.

In figure 2 (right and left panels) we see typical quasinormal mode evolutions for the scalar field for different values of  $l$ : the higher the multipole number, the smaller the frequency of oscillation. The imaginary part of  $\omega$  varies very slowly with  $l$ , which is typical for the Schwarzschild-dS geometry also in the absence of couplings. The interesting feature is the emergence of an oscillatory evolution, introduced by the  $\eta$ -coupling for the  $l = 0$  mode: there is a quasinormal ringing phase (left panel of 2) which does not exist in the dS-Schwarzschild case [42].

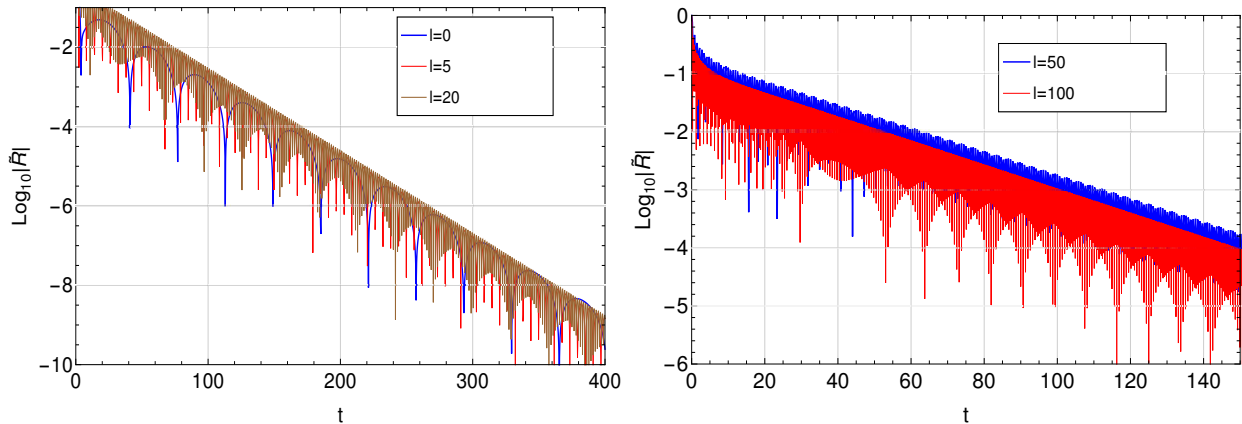


FIG. 2. Time evolution of the scalar field with different values of  $l$  and  $L$ . The parameters of the geometry are  $M = L/6 = m/0.3 = \eta = 1$ .

The effect of the cosmological constant is similar in the Schwarzschild-dS case: the higher the  $\Lambda$ , the smaller the real part of  $\omega$ . The behavior for  $\omega_I$  is more complicated, oscillating in a given scope of  $L$  and becoming arbitrarily small as  $\Lambda$  increases. This can be seen in figure 3 (left panel), and in table III, which lists quasi-frequencies for different values of  $l$  and  $L$ . In the same table we can also see different  $\omega$  for a range of  $\eta$ : the asymptotic values of the coupling are the same as for the massless scalar field propagation in a Schwarzschild-dS Universe.

In the right panel of figure 3 we see the transition between stable/unstable dynamics as a function of  $\eta$  for the special case  $l = 0$ . Stable evolution takes place from  $\eta = 0$  until

$\eta < L^2/3 = 27$ , exhibiting the expected decay in time (the potential being only positive). For  $\eta > L^2/3$ , on the other hand, the dynamics is always unstable: even for  $\eta > \eta^{(1)} \sim 63.28$ , where the potential is partly positive, there is no stable evolution (see right panel of figure 3).

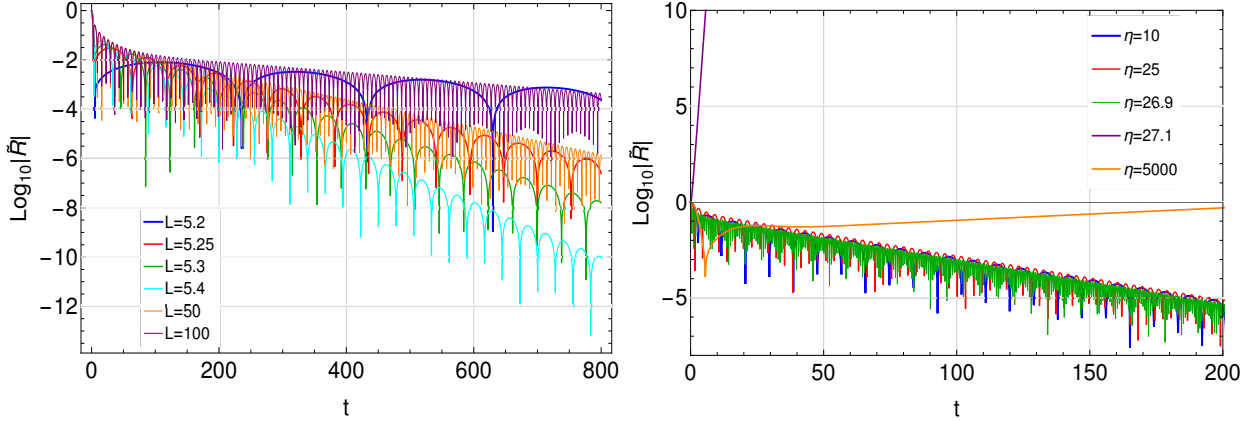


FIG. 3. Time evolution of the scalar field for different values of  $l$  and  $L$ . Geometry parameters read  $M = l = \mu/0.5 = \eta/2 = 1$  (left panel) and  $M = L/9 = m/0.5 = 1$ ,  $l = 0$  (right panel).

TABLE III. Fundamental quasinormal modes for non-minimally coupled scalar field evolving in Schwarzschild-dS black holes.

| $M = \eta = L/6 = m/0.3 = 1$ |                      | $M = l = m/0.5 = \eta/2 = 1$ |                       | $M = l = L/9 = m/0.5 = 1$ |                     |
|------------------------------|----------------------|------------------------------|-----------------------|---------------------------|---------------------|
| $l$                          | $\omega$             | $L$                          | $\omega$              | $\eta$                    | $\omega$            |
| 0                            | $9.695 - 0.04775i$   | 5.2                          | $0.01590 - 0.003730i$ | 0                         | $0.1982 - 0.04479i$ |
| 1                            | $4.909 - 0.04658i$   | 5.25                         | $0.05927 - 0.01367i$  | 5                         | $0.2352 - 0.04397i$ |
| 2                            | $1.977 - 0.04787i$   | 5.3                          | $0.08177 - 0.01876i$  | 10                        | $0.5381 - 0.04349i$ |
| 3                            | $0.5339 - 0.04797i$  | 5.4                          | $0.1131 - 0.02565i$   | 11                        | $0.3907 - 0.04344i$ |
| 4                            | $0.4386 - 0.04792i$  | 6                            | $0.2092 - 0.04446i$   | 50                        | $0.1966 - 0.05852i$ |
| 5                            | $0.3440 - 0.04781i$  | 10                           | $0.3659 - 0.05512i$   | 55                        | $0.1301 - 0.05125i$ |
| 20                           | $0.2506 - 0.04757i$  | 30                           | $0.4469 - 0.02382i$   | 56                        | $0.1105 - 0.5731i$  |
| 50                           | $0.1608 - 0.04688i$  | 50                           | $0.4588 - 0.01281i$   | 500                       | $0.1100 - 0.05751i$ |
| 100                          | $0.08713 - 0.04506i$ | 100                          | $0.4694 - 0.004889i$  | 5000                      | $0.1318 - 0.05088i$ |

This picture changes significantly for  $l > 0$ , as can be seen in figure 4, for  $l = 1$ . The

evolution of the scalar field becomes unstable for a range of  $\eta$  going from  $L^2/3$  to  $\eta_T \sim 31.8$  with the adopted parameter values. This critical value of  $\eta$  lies in the region (iii) of  $V$ ; in the same region, for  $31.8 < \eta < \eta^{(2)} \sim 56.16$ , a very short quasinormal ringing phase forms, and finally the field decays exponentially. This behavior is seen for every  $l > 0$ : since the potential has four different regions, there is always a threshold  $\eta_T$  in the region (iii) above which the field, instead of being unstable, decays in time. The peculiar behavior is the range where we have unstable modes:  $L^2/3 \leq \eta \leq \eta_T$ . In [41], the critical behavior associated with  $\eta$  was found to present a single transition value.

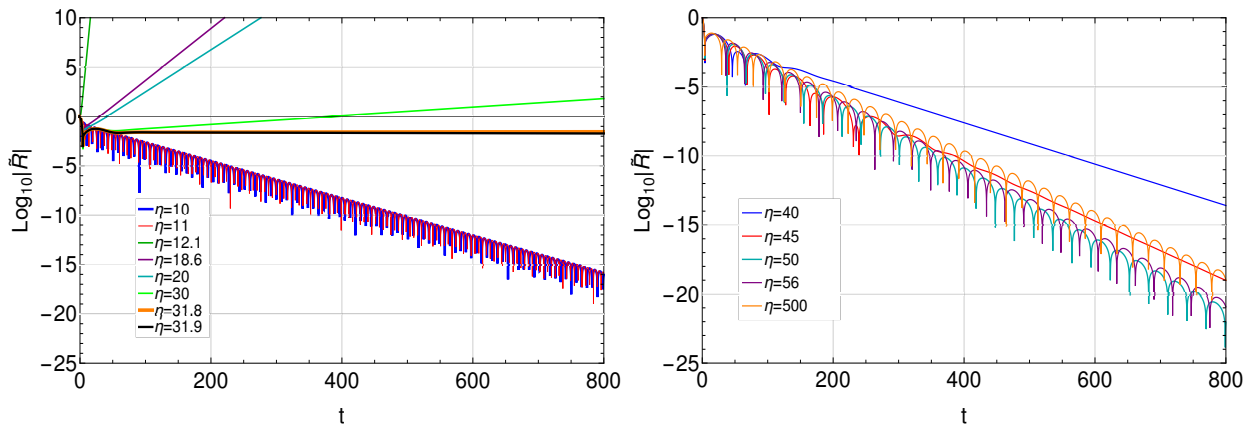


FIG. 4. Time evolution of the scalar field for various values of  $\eta$  and  $M = l = L/6 = \mu/0.5 = 1$ .

In figure 4 the asymptotic tendency for growing  $\eta$  becomes evident: for high values of the coupling, the scalar field tends to decouple as if it freely propagated in the Schwarzschild-dS geometry, without mass.

Regarding the transition from stable to unstable evolutions, the same behavior is observed in the Reissner-Nordstroem geometry, namely a region of instability for  $\eta$ , but in this case also for the mode  $l = 0$ . We explore the subject in the next section.

## V. QNM'S FOR NON-MINIMALLY COUPLED SCALAR FIELD EVOLVING IN REISSNER-NORDSTRÖM-DE SITTER SPACETIME

In a Reissner-Nordström-de Sitter spacetime (RNdS), the line-element has exactly the same form of (18), with

$$f(r) = 1 - \frac{2M}{r} + \frac{Q^2}{r^2} - \frac{r^2}{L^2}. \quad (37)$$

The functions related to the Klein-Gordon equation as found in (10) can be written as

$$\alpha = f^2, \quad \beta = f \left( 1 + \frac{2Q^2 \eta}{r^4 k} \right), \quad \gamma = \frac{f}{k}, \quad F = \ln(kf), \quad (38)$$

where

$$k = k(r, Q, L, \eta) = 1 + \eta B = 1 - \frac{3\eta}{L^2} - \frac{\eta Q^2}{r^4}. \quad (39)$$

In order to separate variables and eliminate the radial first derivative from the wave equation, we must choose a non-trivial field transformation, different from the one used for the well-known Schwarzschild case (equation (33)), namely

$$R \rightarrow \frac{\tilde{R}}{r\sqrt{k}}. \quad (40)$$

Together with the tortoise coordinate system, this transformation sets the Klein-Gordon equation in the same simple form of (34). As a drawback, it introduces a discontinuity in the field at the point  $k(r)|_{r=r_d} = 0$ , which poses numerical difficulties. We only consider cases where  $r_d$  is encapsulated by a horizon and is, therefore, of no consequence.

From the four roots of  $f(r)$ , at least one is negative, if two or more real roots exist. We restrict ourselves to the study of a geometry with 3 different horizons, namely, Cauchy  $r_y$ , event  $r_h$  and cosmological horizon  $r_c$ , with  $r_y < r_h < r_c$ . As in the Schwarzschild case, the evolution of the scalar field takes place in a region  $\mathbb{X}$  defined by  $\mathbb{X} : r_h < r < r_c$ . Taking  $a \equiv \frac{Q}{M} > 0$ , there are two possible conditions with 3 different positive solutions for  $f(r) = 0$ ,

$$(i) \quad \frac{1}{L^2} < \frac{p_+(a)}{32M^2} \quad \text{and} \quad a < 1; \quad \text{or} \\ (ii) \quad \frac{p_-(a)}{32M^2} < \frac{1}{L^2} < \frac{p_+(a)}{32M^2} \quad \text{and} \quad 1 < a < \sqrt{9/8},$$

where  $p_{\pm}(a) = [-27 + 36a^2 - 8a^4 \pm (9 - 8a^2)^{3/2}] / a^6$ . The condition (i) recovers the Schwarzschild limit for  $a \rightarrow 0$ , as stated in [42], with 2 different horizons. The condition (ii) appears as a limit situation in [47].



### A. Effective Potential

Given the field transformation (40) and the metric functions defined above, the effective potential for the scalar field reads

$$\begin{aligned} \tilde{V}(r) = f \left[ \frac{2rk k'' + 4kk' - rk'^2}{4rk^2} f + \frac{2k + rk'}{2rk} f' + \left( 1 + \frac{2Q^2\eta}{r^4k} \right) \frac{l(l+1)}{r^2} + \frac{m^2 + \xi\mathcal{R}}{k} \right] = \\ \frac{f}{k} \left[ \frac{2\eta Q^2(9\eta r^4 + \eta L^2 Q^2 - 3L^2 r^4)}{r^6(-3\eta r^4 - \eta L^2 Q^2 + L^2 r^4)} \left( 1 - \frac{2M}{r} + \frac{Q^2}{r^2} - \frac{r^2}{L^2} \right) \right. \\ \left. + \left( \frac{\eta Q^2 + r^4 - 3\eta r^4/L^2}{r^5} \right) \left( \frac{2M}{r^2} - \frac{2Q^2}{r^3} - \frac{2r}{L^2} \right) + \left( 1 - \frac{3\eta}{L^2} + \frac{\eta Q^2}{r^4} \right) \frac{l(l+1)}{r^2} + \frac{12\xi}{L^2} + m^2 \right]. \end{aligned} \quad (41)$$

Here the Ricci term plays no special role in the coupling with the scalar field and can be rescaled as part of the mass field such as  $\mu^2 = \xi\mathcal{R} + m^2$ . Thus, the Ricci scalar is not directly related to the presence or absence of unstable modes of the scalar field.

In the limit  $Q = 0$ , the coupled-Schwarzschild potential is recovered. We do not concern ourselves with the point of discontinuity,

$$r = r_d|_{k(r)=0} = \left( \frac{\eta Q^2}{1 - 3\eta/L^2} \right)^{1/4}, \quad (42)$$

since it originates from our choice of field transformation; we restrain ourselves to one of the ranges:  $r_d < r_h$  or  $r_c < r_d$ , such that  $r_d$  is either encapsulated by the event horizon or outside the cosmological horizon.

Let us consider as an example the massless scalar field, with parameters  $M = 5Q/3 = (L/5.4)^2 = l/2 = 1$ . In this situation, the potential in  $\mathbb{X}$  can be divided, according to its signal, in the five different regions as described in table IV. A different situation arises, however, when the charge exceeds a critical value  $Q_c$ . For  $M = l/2 = (L/6)^2 = 1$ , and  $\mu^2 = 0$ , for instance, if  $Q > Q_c \sim 0.852$ , then even for high  $\eta$  values, region (v) does not occur. For  $Q = 0.86$ , the potential can be divided in the regions shown in table V. Plots for under- and super-critical behaviors are shown in figure 5.

The existence of a critical value  $Q_c$  is stable against changes in  $\mu$  and  $l$ : for every pair  $(l, \mu)$  when  $Q < Q_c$  we can always find a sufficient high  $\eta_k$  such that for any  $\eta > \eta_k$  we have  $V_{\mathbb{X}} > 0$ ; on the other hand, for  $Q > Q_c$  the potential is strictly negative in  $\mathbb{X}$ .

Considering the different character of the potential for the cases (i) to (v), we can investigate the field evolution by obtaining the system's quasinormal modes and determining

TABLE IV. Different regions for the potential in RNdS, with  $M = 5Q/3 = (L/5.4)^2 = l/2 = 1$ .

| Case  | $\eta$ -range                       | Signal of $V_{\mathbb{X}}$ | $r_d$             |
|-------|-------------------------------------|----------------------------|-------------------|
| (i)   | $\eta \lesssim 8.46$                | $V_{\mathbb{X}} > 0$       | $r_d < r_h$       |
| (ii)  | $8.46 \lesssim \eta \lesssim 9.56$  | $V_{\mathbb{X}} \geq 0$    | $r_h < r_d < r_c$ |
| (iii) | $9.56 \lesssim \eta \lesssim 9.88$  | $V_{\mathbb{X}} < 0$       | $r_c < r_d$       |
| (iv)  | $9.88 \lesssim \eta \lesssim 11.52$ | $V_{\mathbb{X}} \geq 0$    | $r_c < r_d$       |
| (v)   | $11.52 \lesssim \eta$               | $V_{\mathbb{X}} > 0$       | $r_c < r_d$       |

TABLE V. Different regions for the potential in RNdS, for  $Q = 0.86 > Q_c$  (and  $M = l/2 = (L/6)^2 = 1; \mu^2 = 0$ ).

| Case  | $\eta$ -range                        | Signal of $V_{\mathbb{X}}$ | Place of $r_d$    |
|-------|--------------------------------------|----------------------------|-------------------|
| (i)   | $\eta \lesssim 5.84$                 | $V_{\mathbb{X}} > 0$       | $r_d < r_h$       |
| (ii)  | $5.84 \lesssim \eta \lesssim 11.78$  | $V_{\mathbb{X}} \geq 0$    | $r_h < r_d < r_c$ |
| (iii) | $11.78 \lesssim \eta \lesssim 12.23$ | $V_{\mathbb{X}} < 0$       | $r_c < r_d$       |
| (iv)  | $12.23 \lesssim \eta$                | $V_{\mathbb{X}} \geq 0$    | $r_c < r_d$       |

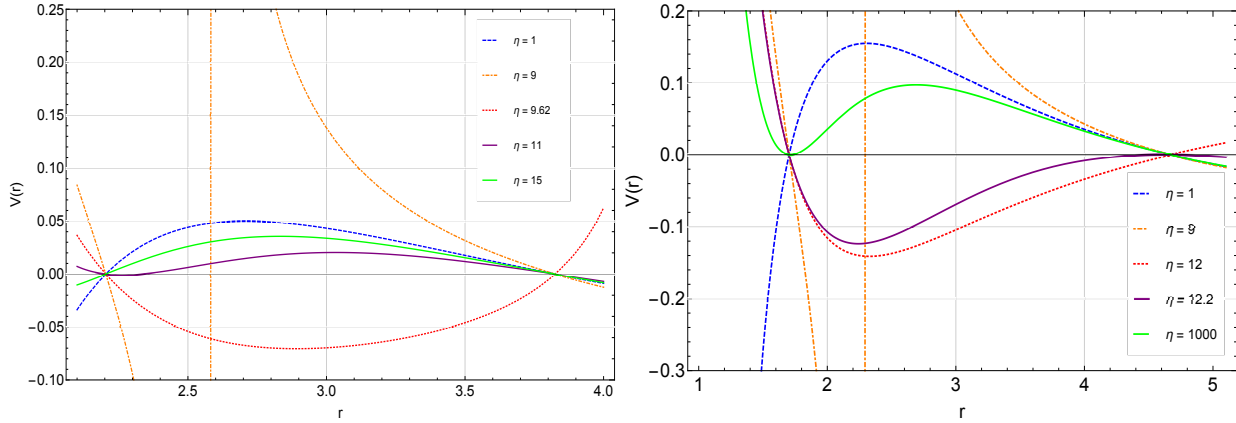


FIG. 5. Potential of the Klein-Gordon field in the RNdS geometry with non-minimally coupling. Left panel: Potential for the regions (i) ( $\eta = 1$ ) to (v) ( $\eta = 15$ ) of table IV. The horizons are located at  $r_h/2.204 = r_c/3.825 = 1$ . Right panel: Potential for regions (i) to (iv) of table V. The two last  $\eta$  lie on region (iv). The horizon locations are  $r_h/1.703 = r_c/4.669 \sim 1$ .

whether unstable evolutions are present, or investigate the late time (after the quasinormal

ringing). For this reason, we choose to use the characteristic integration over null coordinates to obtain the field profiles together with pony method for the quasi-frequencies. For strictly positive gaussian-like potentials, we compare the frequencies to those obtained with WKB method, with good agreement between the results.

## B. Evolution of scalar field and QNM's

The typical evolution of a scalar field coming from the Klein-Gordon equation can be seen in figure 6 for  $r = 2r_h$  and different values of  $Q$ . For the chosen parameters,  $V_{\mathbb{X}} > 0$  and, as anticipated, there are no instabilities: all profiles decay exponentially in time. Higher values of the charge, however, lead to  $V_{\mathbb{X}}$  being partly positive and partly negative, allowing for unstable modes to arise.

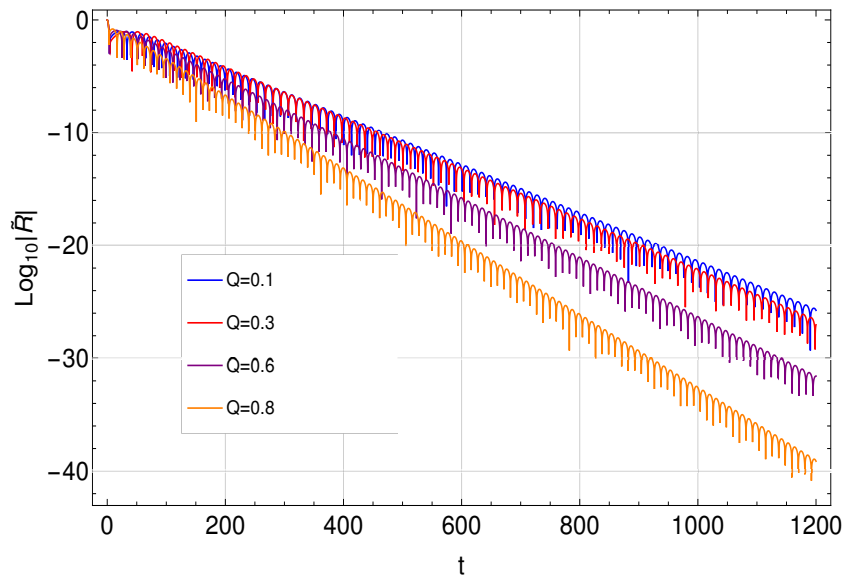


FIG. 6. Scalar field propagation in a RNdS black hole with non-minimal coupling. The constant parameters read  $M = L^2/36 = l/2 = \eta/50 = 1$ ,  $\mu^2 = 0$ , resulting in  $V_{\mathbb{X}} > 0$ .

With the acquired quasinormal signal and the prony method [48] we obtain the fundamental quasinormal frequencies up to the critical value of charge  $Q_c \sim 0.85$ , as listed in the table VI. The obtained frequencies are significantly different from the case with no couplings, where, with the chosen parameters and  $\eta = 0$ , typically  $\omega \sim 0.5 + 0.09i$ . The quasi-frequencies with coupling display a behavior similar to that of the RNdS case (coupling

absent): the increase in the charge causes a pronounced growth in the imaginary part and a mild one in the real part.

TABLE VI. Fundamental quasinormal modes for non-minimally coupled scalar field evolving in RNdS black holes with different values of  $Q$ . The spacetime parameters read  $M = L/6 = l/2 = \eta/50 = 1$  and  $\mu^2 = 0$ .

| $Q$  | $\text{Re}(\omega)$ | $\text{Im}(\omega)$ | $Q$  | $\text{Re}(\omega)$ | $\text{Im}(\omega)$ |
|------|---------------------|---------------------|------|---------------------|---------------------|
| 0.05 | 0.2338              | -0.04905            | 0.50 | 0.2581              | -0.05667            |
| 0.10 | 0.2346              | -0.04927            | 0.55 | 0.2624              | -0.05849            |
| 0.15 | 0.2360              | -0.04963            | 0.60 | 0.2667              | -0.06064            |
| 0.20 | 0.2379              | -0.05015            | 0.65 | 0.2710              | -0.06627            |
| 0.25 | 0.2402              | -0.05081            | 0.70 | 0.2751              | -0.06318            |
| 0.30 | 0.2431              | -0.05163            | 0.75 | 0.2792              | -0.07003            |
| 0.35 | 0.2463              | -0.05261            | 0.80 | 0.2836              | -0.07457            |
| 0.40 | 0.2500              | -0.05377            | 0.85 | 0.2884              | -0.08017            |

In figure 7 we find two field profiles nearby  $Q \sim Q_c$  (upper-left panel) and the instabilities found for high values of  $Q$  (upper-right, lower-left panels). We can see in the same figure (right-bottom panel) the stability of the near extremal black hole to the scalar field (an expected result, since the potential is strictly positive in  $\mathbb{X}$ ). The existence of negative regions in the potential does not ensure the presence of instabilities; otherwise, the negativity on  $V_{\mathbb{X}}$  is related to the presence of an exponential decay in the long-time profile domain. Before  $Q_c$ , the field oscillates indefinitely (right panel in figure 7,  $Q = 0.85$ ), and beyond this critical charge an exponential decay is shaped as seen in many dS-like geometries [49, 50] (upper-right panel in figure 7). The exponential decay takes place from  $Q_c$  to another high value of  $Q$ , namely  $Q \sim 0.907$  for the assigned parameters (upper-right panel). For  $Q \gtrsim 0.907$  and undercharged black holes ( $Q < M$ ), the field growth is unlimited (figure 7 bottom-left panel). In this case we may not assume the geometry preserves its original shape: it may evolve to a distinct form. The right panel on the bottom represents a near-extreme black hole with  $\eta$ : we can see again the indefinite oscillations typical from a dS-like geometry near the quasi-extreme regime. Finally, when the black hole overpasses the value  $Q = M$ , the scalar field evolves as the usual damped oscillator. This transitional behavior seems

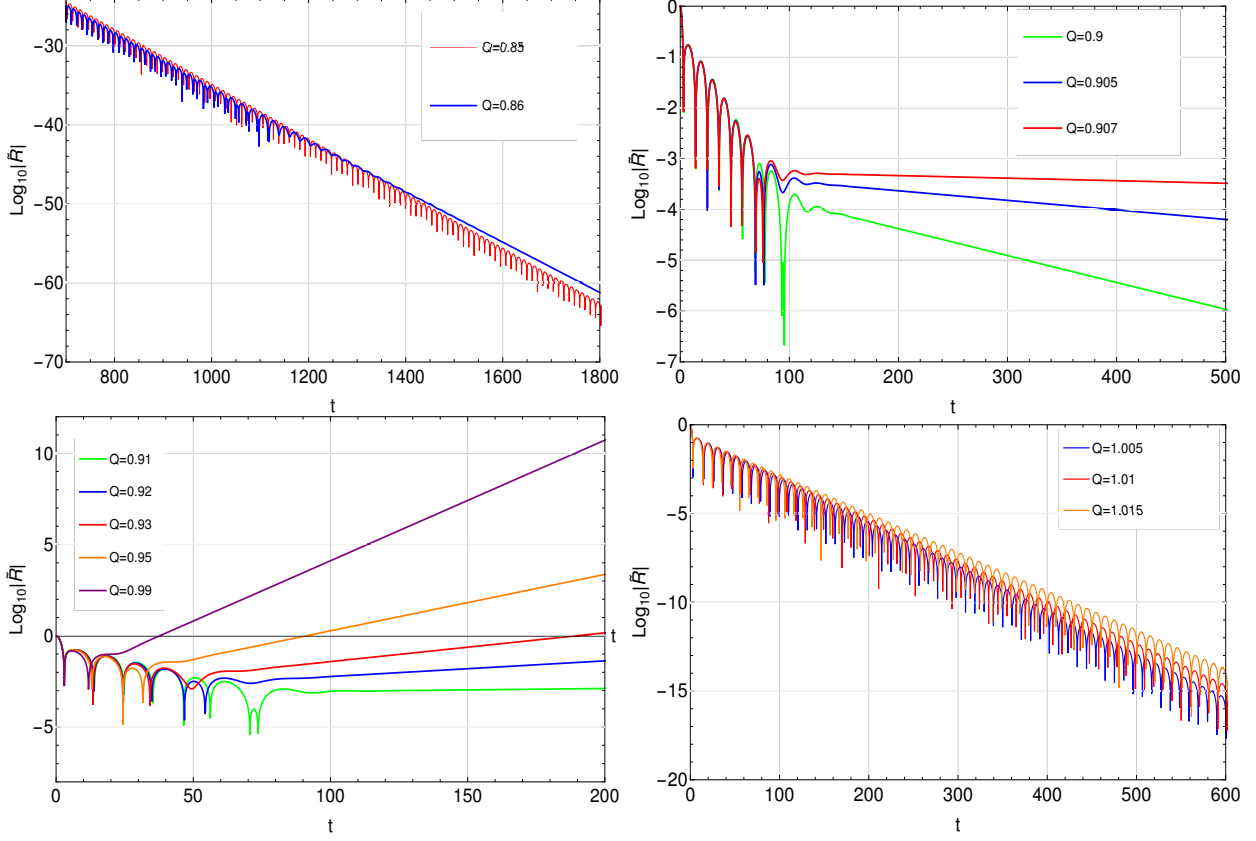


FIG. 7. Field profile with parameters  $M = L^2/36 = 1$ ,  $\mu^2 = 0$ ,  $\eta/25 = l = 2$  (upper and lower left profiles) or  $\eta = l = 1$  (bottom right). The instabilities in the field arise as a result of the mixed potentials (negative and positive) for large enough  $Q$ 's. In the upper-left panel the field was put to evolve from  $R = 1, t = 0$ , decaying as expected. For  $Q = \sqrt{9/8} \sim 1.0156$ , we have  $r_c = r_h$ .

to be general: it does not disappear with varying  $\eta$  or other black holes parameters. To demonstrate this, by taking fixed  $M, Q$  and  $L$  we vary the  $\eta$ -parameter and investigate the presence of quasinormal modes in regions (i) to (v), with the same strategy. In figure 8 we see different profiles for a large range of  $\eta$ .

In the upper-left panel of figure 8 we see the field propagation, with  $\eta$ -parameter in the region (i), until  $\eta^{(1)} \sim 13.29$ : the signal damped-oscillates as a never-ending evolution. There are no unstable profiles in this region. From  $\eta \sim 13.29$  to  $\eta \sim 16.27$  the potential is not continuous (region (ii)). Region (iii), however, is the most critical for the scalar field (since  $V_{\mathbb{X}} < 0$  there) and presents the most unstable region. On the upper-right panel we see two profiles with  $\eta \sim 16.3$  and  $\eta \sim 16.35$ , both unstable. The rapidly exponential growth comes

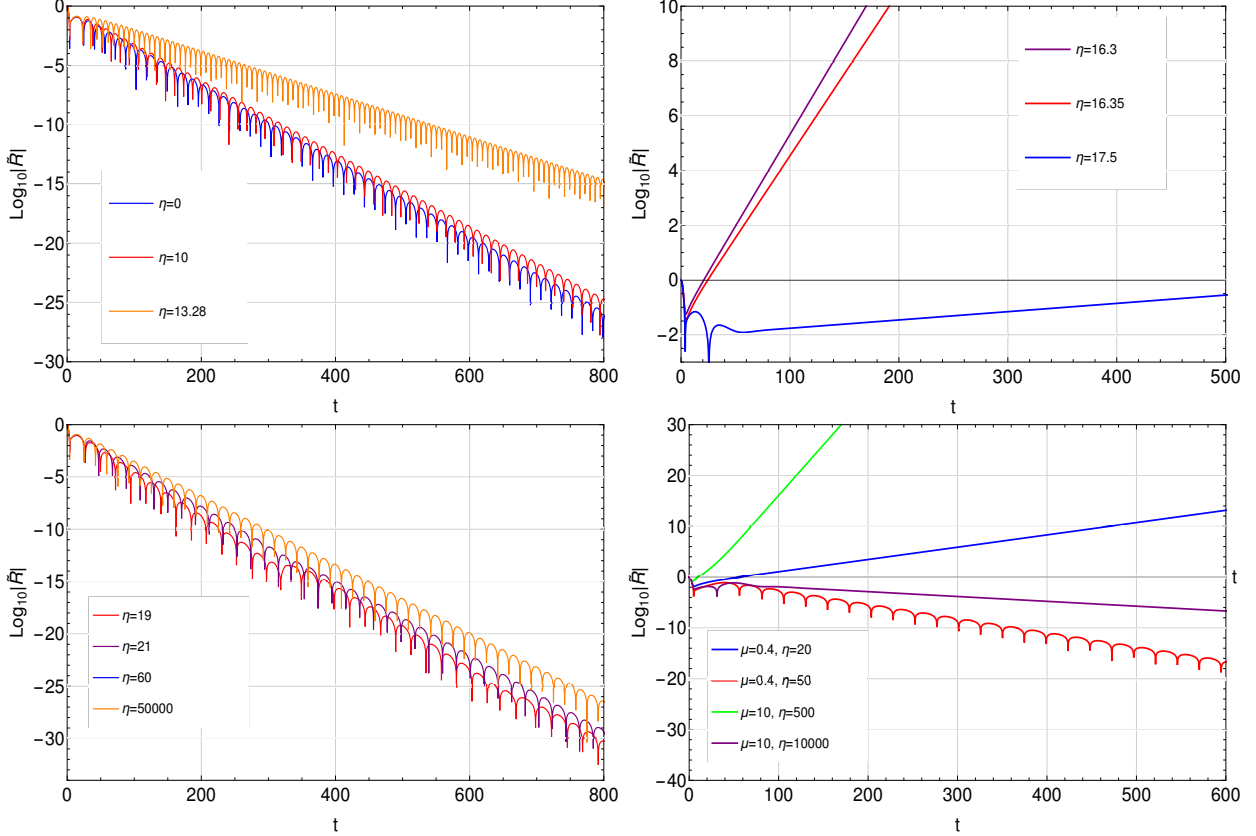


FIG. 8. Field profile with parameters  $M = l = 2Q = L^2/49 = 1$  and  $\mu^2 = 0$ . From upper-left to lower-right, we see the emergence of unstable fields in an intermediate region ((iii) and (iv)) of the  $\eta$  parameter. The critical charge related to the formation of region (v) for the chosen parameters is  $Q_c \sim 0.777$ . In the lower-right panel we see the massive field profile with coupling.

from the fact that  $V_{\mathbb{X}} < 0$  for almost every  $r \in \mathbb{X}$ . The fourth region begins at  $\eta^{(2)} \sim 16.3985$  going to a maximum value  $\eta^{(3)} \sim 21.17$ : we can see different field profiles in the upper-right and lower-left panels stable/unstable, depending on the parameter. The transition from stable to unstable profiles takes place nearby  $\eta \sim 17.6$ , still in region four: both kinds of signal occur, depending on how negative the potential is. After  $\eta \sim 21.17$  (lowerleft-panel) we see the last two quasinormal modes (region (v)), as never-ending damping oscillating signals. In the high  $\eta$  regime, the field profile approaches the absent coupling case and oscillates following closely the Reissner-Nordstroem-de Sitter record.

Considering the variation of  $l > 0$  for different  $\eta$ , the general behavior in the potential is the raising of its peak, which does not relate to the formation of stable asymptotic regions

(region (v)). Otherwise, this fact is related to the range at which we have unstable modes: the higher the multipole number, the more stable the scalar field tends to perform.

If we take high values of cosmological radius, we may see again a significant range of the  $\eta$ -parameter for which the scalar field profile oscillates indefinitely, and no unstable modes form. As an example, let us assume a geometry with  $M = l = 1$ ,  $\mu = 0$  and  $L = 60000$ . The value of  $\eta^{(3)}$  happens nearby  $\sim 4.8 \cdot 10^9$  from which region (v) forms. It forms however, for very small values of charges,  $Q < Q_c \sim 10^{-4}$ . The region for negative potential almost vanishes: it endures a range of  $\Delta\eta \sim 0.00001$ . After that, there is also a small range in  $\eta$  for instabilities and then, all modes come out stable.

The situation changes drastically, though, if we add a small scalar field mass to the last scenario. Taking  $\mu \sim 0.1$ , as an example, we have a range  $\Delta\eta \sim 10^9$  of unstable fields after the point  $\eta^{(2)} \sim 1.2 \cdot 10^9$ .

In figure 8 in lower-right panel we see the coupling of  $\eta$  and the scalar field: in general, the higher the scalar field mass, the higher the value of  $\eta$  for the formation of a stable region of oscillations in the potential.

We will end this work studying the near extremal black hole in next section for the special case of a Schwarzschild black hole.

## VI. QNM'S FOR NON-MINIMALLY COUPLED SCALAR FIELD EVOLVING IN QUASI-EXTREMAL SCHWARZSCHILD-DE SITTER BLACK HOLES

The quasinormal modes for a massive scalar field minimally coupled evolving in Schwarzschild-dS black holes in the quasi-extremal limit (defined by  $\delta = \frac{r_c - r_+}{r_+} \ll 1$ ) have been exactly and numerically calculated by Molina [50], and Cardoso and Lemos [49]. Following their approach we extend the calculation for the non-minimally coupled case. The effective potential can be written in terms of the tortoise coordinate  $r_*$  as

$$V(r_*) = \frac{V_0}{\cosh^2(\kappa_+ r_*)} \quad (43)$$

where  $\kappa_+ = \frac{1}{2} \frac{df}{dr} |_{r=r_+}$  is the surface gravity at the event horizon  $r_+$  and  $V_0$  is the settle [ponto de sela? entao “saddle point”] point of  $V(r)$  given by

$$V_0 = \left[ \frac{\ell(\ell + 1)}{r_+^2} + \frac{\mu^2 L^2}{L^2 - 3\eta} \right] \frac{(r_c - r_+) \kappa_+}{2}. \quad (44)$$

In Fig.(9) we see the effective potential for different values of  $\eta$  and  $\ell$ . If the well is deep enough, unstable modes appear. This effective potential (43) is similar to the Poschl-Teller

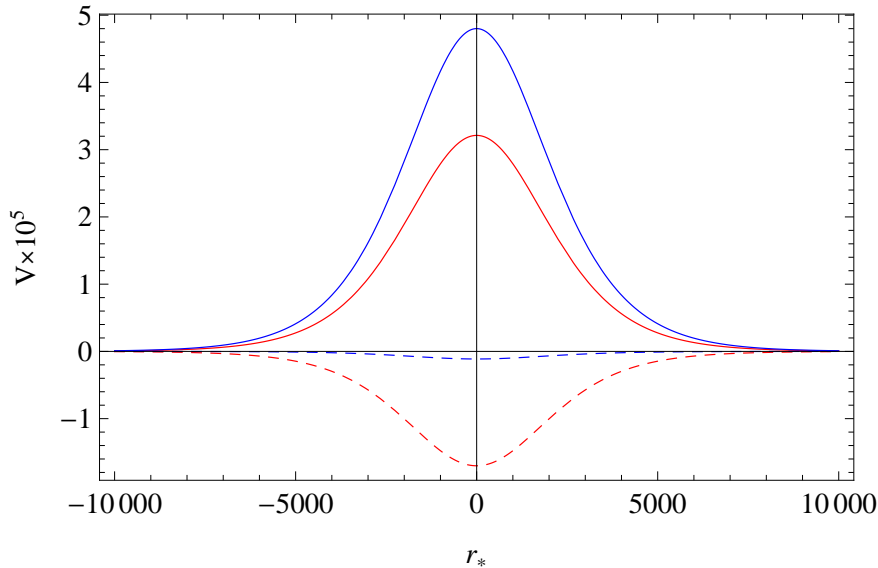


FIG. 9. Effective potential for a quasi-extremal SdS black hole with  $L = 25.98$  and  $M = 5.0$ . The mass of scalar field is fixed in  $\mu = 1$ . The blue and red lines with  $\eta = 0$  (straight) and  $\eta = 650$  (dashed) represent the potentials for  $\ell = 0$  ( $\ell = 10$ , respectively).

potential for which the QNM's can be exactly obtained with appropriated boundary conditions [49, 50]. The expression is given by

$$\omega = \kappa_+ \left[ \sqrt{\frac{V_0}{\kappa_+^2} - \frac{1}{4}} - i \left( n + \frac{1}{2} \right) \right], \quad (45)$$

where  $R(r, t) = \tilde{R}(r)e^{-i\omega t}$ . Substituting Eq. (44) into the Eq. (45), the QNM's for massive non-minimally coupled scalar field in quasi-extremal Schwarzschild-de Sitter black holes can be written in terms of  $(\ell, \mu, \eta)$  and the characteristic parameters of the black holes  $(r_+, r_c, \kappa_+)$  as follows

$$\frac{\omega}{\kappa_+} = \sqrt{\left[ \frac{\ell(\ell+1)}{r_+^2} + \frac{\mu^2 L^2}{L^2 - 3\eta} \right] \frac{r_c - r_+}{2\kappa_+} - \frac{1}{4}} - i \left( n + \frac{1}{2} \right). \quad (46)$$

In Tables VII and VIII we present the general behavior for the QNM's for two different quasi-extremal Schwarzschild-dS black holes, obtained from the Eq. (46) with varying  $\eta$ . Transitions between three possible different regimes can be seen. For  $0 < \eta < \eta_{\text{critical}}$  the system is in a stable regime since the imaginary part of the QNM's is negative and constant



and the frequencies of oscillation increase rapidly near to  $\eta_{\text{critical}}$ . For  $\eta_{\text{critical}} < \eta < \eta_{\text{stableII}}$  the system becomes unstable with a positive purely imaginary QNM which decreases and goes to zero at  $\eta_{\text{stableII}}$ . When  $\eta_{\text{stableII}} < \eta < \eta_{\text{stableIII}}$  the system returns to a stable regime with an exponential decay. Beyond  $\eta_{\text{stableIII}}$  the system is still stable but now with an oscillatory exponential decay. In this case, the imaginary part of the QNM's is constant and the frequencies of oscillation tend to a constant.

TABLE VII. Quasi-normal modes for non-minimally coupled scalar field evolving in quasi-extremal SdS black holes for several values of  $\eta$  and  $\ell = 1, \mu = 1, n = 3$ .

| $M = 5.0, \quad L = 25.982, \quad \delta = 0.01$ |   |   | $M = 10.0, \quad L = 51.97, \quad \delta = 0.02$ |   |   |
|--|---|---|--|---|---|
| $\eta$   | $\text{Re}\left(\frac{\omega}{\kappa_+}\right)$ | $\text{Im}\left(\frac{\omega}{\kappa_+}\right)$ | $\eta$   | $\text{Re}\left(\frac{\omega}{\kappa_+}\right)$ | $\text{Im}\left(\frac{\omega}{\kappa_+}\right)$ |
| 100  | 22.7587   | -3.5  | 100  | 33.6568   | -3.5  |
| 220  | 101.159   | -3.5  | 900  | 1667.29   | -3.5  |
| 230  | 0.  | 96.9866   | 1000   | 0.  | 86.352  |
| 400  | 0.  | 9.88087   | 2000   | 0.  | 21.5867   |
| 670  | 0.  | -1.82693  | 8000   | 0   | -2.05361  |
| 30000  | 10.4745   | -3.5  | 50000  | 9.8107  | -3.5  |
| $\infty$   | 10.5557   | -3.5  | $\infty$   | 10.6242   | -3.5  |

TABLE VIII. Quasi-normal modes for non-minimally coupled scalar field evolving in quasi-extremal SdS black holes for several values of  $\eta$  and  $\ell = 0, \mu = 1, n = 0$ .

| $M = 5.0, \quad L = 25.982, \quad \delta = 0.01$ |   |   | $M = 10.0, \quad L = 51.97, \quad \delta = 0.02$ |   |   |
|--|---|---|--|---|---|
| $\eta$   | $\text{Re}\left(\frac{\omega}{\kappa_+}\right)$ | $\text{Im}\left(\frac{\omega}{\kappa_+}\right)$ | $\eta$   | $\text{Re}\left(\frac{\omega}{\kappa_+}\right)$ | $\text{Im}\left(\frac{\omega}{\kappa_+}\right)$ |
| 100  | 20.1566   | - 0.5   | 100  | 31.932  | - 0.5   |
| 220  | 100.606   | - 0.5   | 900  | 1667.25   | - 0.5   |
| 230  | 0.  | 100.541   | 1000   | 0.  | 89.9793   |
| 400  | 0.  | 16.5505   | 2000   | 0.  | 26.7483   |
| 670  | 0.  | 10.1991   | 8000   | 0.  | 10.2339   |
| 30000  | 0.  | 0.898929  | 50000  | 0.  | 3.60777   |
| $\infty$   | 0.  | 0.  | $\infty$   | 0.  | 0.  |

In the high coupling limit ( $\eta \rightarrow \infty$ ) the QNM's are

$$\frac{\omega_\infty}{\kappa_+} = \sqrt{\ell(\ell+1) - \frac{1}{4}} - i \left( n + \frac{1}{2} \right), \quad (47)$$

becoming independent of the effective mass  $\mu$ . In this limit, for  $\ell = 0$  the modes become purely imaginary  $\frac{\omega_\infty}{\kappa_+} = -in$ , and the fundamental mode ( $n = 0$ ) to vanishes.

The behavior of QNM's for different overtones and multipoles are illustrated in figure 10. The temporal evolution of the scalar field in the quasi-extremal Schwarzschild-de Sitter is presented in the figure 11.

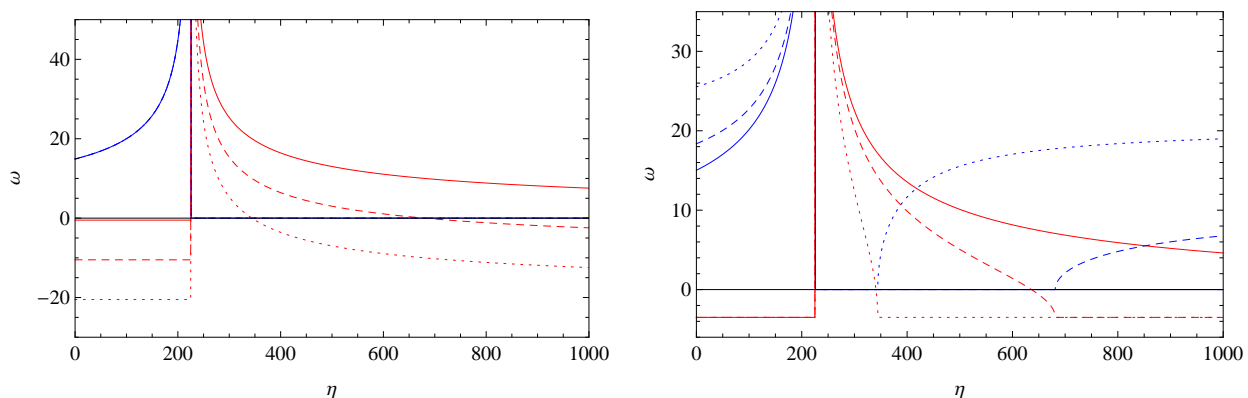


FIG. 10. Quasinormal modes for non-minimally coupled scalar field evolving in quasi-extremal SdS black holes with  $L = 25.98$ ,  $M = 5.0$  and  $\mu = 1$ . The blue and red lines represent  $\text{Re}(\omega)$ , and  $\text{Im}(\omega)$ , respectively. In the left panel the fundamental mode (straight) and the overtone  $n = 10$  (dashed) are presented, and  $n = 20$  (dotted) with  $\ell = 0$ . In the right panel, overtone  $n = 3$  with the following multipoles  $\ell = 0$  (straight),  $\ell = 10$  (dashed), and  $\ell = 20$  (dotted) are found.

The critical coefficients of  $\eta$  stand for  $\eta_{\text{critical}} = \frac{L^2}{3}$ ,

$$\eta_{\text{stableII}} = \frac{L^2}{3} + \frac{L^2 \mu^2 r_+^2 \delta_+}{3n(1+n)r_+^2 + 3\ell(\ell+1)\delta_+} \quad \text{if } (n \neq 0, \ell \neq 0) \quad (48)$$

where  $\delta_+ = \frac{r_c - r_+}{2\kappa_+}$ , and

$$\eta_{\text{stableIII}} = \frac{L^2}{3} - \frac{4L^2 \mu^2 r_+^2 \delta_+}{3(r_+^2 - 4\ell(\ell+1)\delta_+)} \quad (49)$$

If  $n \neq 0$  and  $\ell = 0$  then  $\eta_{\text{stableIII}} < \eta_{\text{stableII}}$  and there is no oscillatory exponential decay. If  $n = \ell = 0$ , then the system does not form an unstable regime since  $\eta_{\text{stableII}} \rightarrow \infty$ , i.e., this fundamental mode is unstable to  $\eta > \eta_{\text{critical}}$ . The fundamental mode with no angular momentum, exhibits only two regimes: stable ( $\eta < \eta_{\text{critical}}$ ) or unstable ( $\eta > \eta_{\text{critical}}$ ).

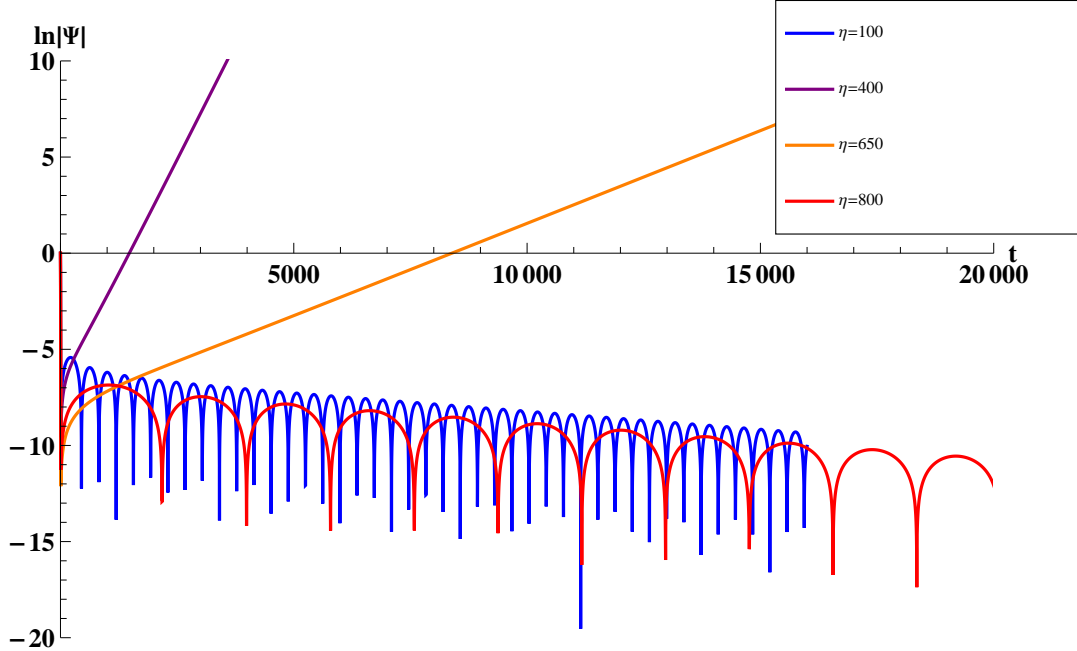


FIG. 11. Field profile in quasi-extremal SdS black holes with  $L = 25.98$ ,  $M = 5.0$ ,  $\mu = 1$  and  $\ell = 10$ .

## VII. FINAL REMARKS

In the present work we discussed the effect of a non-minimally derivative coupling on the dynamics of a scalar field propagating in asymptotically dS spacetimes. Three different cases were studied: the de Sitter, Schwarzschild-de Sitter, and Reissner-Nordström-de Sitter metrics.

Considering the evolution of a scalar probe field in a four-dimensional dS spacetime, we computed the quasinormal spectrum when the NMC term  $\eta$  is present. We found growing quasinormal modes in the positive branch of frequencies leading to regions of instability. In the context of dS/CFT correspondence, we generalize the result for the two-point Hadamard function, showing that its poles match with the regions of instability in the quasinormal spectrum.

In the case of Schwarzschild-de Sitter geometry, the presence of a non-minimally coupled term in the field equation also introduces instabilities in the quasinormal spectra for a given range of  $\eta$ . In particular, the fundamental mode with  $l = 0$  is the most unstable one, with

all oscillations in the range  $\eta > \eta^{(1)}$  being unstable. Differently from the Schwarzschild-de Sitter picture where the scalar field rapidly evolves to a constant, a dynamical evolution is introduced with  $l = 0$  and  $\eta < L^2/3$ : the field evolution displays a quasinormal ringing phase followed by an exponential decay. When  $l > 0$ , unstable modes occur in the range  $L^2/3 < \eta < \eta_T$  in which  $\eta_T$  scales as

$$\eta_T \sim \frac{L^2}{3} \left[ 1 + \frac{\mu^2 L^2}{l(l+3)} \right] \quad (50)$$

for small  $\Lambda$ . The expression above is very similar to (48) for  $n = 0$  and  $L \sim r_+$ , in the quasi-extremal regime.

Surprisingly, the massless scalar field equation is not affected by the coupling. The spectra of frequencies is stable, as expressed by the usual Schwarzschild-de Sitter quasinormal modes. This was shown to be the case also in the de Sitter spacetime (the massless scalar field is unaffected by the NMC coupling).

The same is not true for the Reissner-Nordström black hole in a dS geometry, where even the massless scalar field is affected for the non-minimally coupling constant. The potential is significantly more complicated, compared to the chargeless case, possessing five qualitative different regions according to its sign. In regions (iii) and (iv) we have two critical constants,  $\eta^{(2)}$  and  $\eta^{(3)}$ , determined by the spacetime parameters, such that for  $\eta^{(2)} < \eta < \eta^{(3)}$  unstable modes are present. The range of  $\eta$  for which unstable modes are present grows as we increase the charge of the black hole.

A range of instability for  $\eta$  occurs for every  $l$ , and does not couple specifically to it (differently from [41]). The frequencies are sensitive to the variation of the  $\eta$ -parameter, with the quasinormal spectrum being particularly affected by its presence. The transition to stable regions in the Reissner-Nordström case is not especially influenced by the angular momentum of the wave (contrary to the Schwarzschild case, where  $l = 0$  produces only unstable modes for  $\eta > \eta_T$ ).

For every  $\eta$  it is always possible to find a range of charges of the black hole for which unstable modes are present, suggesting  $\eta$  might be an appropriate order parameter for studying critical phenomena in these systems.

In the quasi-extremal limit for Schwarzschild-de Sitter, the quasi-normal spectra was obtained exactly, following the approach of [49, 50], and the observed behavior is similar to that of the non-quasi-extremal case.

The investigation of the presence of instabilities is a fruitful field of research. In this work, the peculiar evolution of probe fields in a number of geometries revealed critical phenomena which may be related to second order phase transitions present in the corresponding CFT side of theory. Non-minimally coupled models enable a vast amount of dynamical field analysis, with parameter ranges over which the spacetime is unstable being a particularly important feature.

## VIII. ACKNOWLEDGMENTS

The authors would like thank Jefferson Stafusa Elias Portela for critical comments to the manuscript. This work was supported by CNPq (Conselho Nacional de Desenvolvimento Científico e Tecnológico), FAPESP (Fundação de Amparo à Pesquisa do Estado de São Paulo) and FAPEMIG (Fundação de Amparo Pesquisa do Estado de Minas Gerais), Brazil.

### Appendix A: Einstein's tensor components and Ricci scalar for a four-dimensional spherically symmetric spacetime

The Einstein tensor  $G^{\mu\nu}$  has only the diagonal components that can be written in terms of the components of the metric and functions  $A(r)$ ,  $B(r)$  and  $C(r)$ . The non-vanishing components of the Einstein tensor for a spherically symmetric static spacetime can be put in a general form

$$G^{tt} = \frac{A}{f} = \frac{1}{f} \left[ \frac{(1-f)}{r^2} - \frac{f'}{r} \right] \quad (\text{A1})$$

$$G^{rr} = Bf = -f \left[ \frac{(1-f)}{r^2} - \frac{f'}{r} \right] \quad (\text{A2})$$

$$G^{\theta\theta} = \frac{C}{r^2} = \frac{1}{r^2} \left[ \frac{f'}{r} + \frac{f''}{2} \right] = \sin(\theta)^2 G^{\phi\phi}, \quad (\text{A3})$$

and the Ricci scalar is given by

$$\mathcal{R} = - \left( f'' + \frac{4f'}{r} + \frac{2(f-1)}{r^2} \right). \quad (\text{A4})$$

## 1. SdS

In this case the Einstein tensor  $G^{\mu\nu}$  has a simple form and can be written as

$$G^{\mu\nu} = -\frac{3}{L^2} \begin{bmatrix} -\frac{1}{f(r)} & 0 & 0 & 0 \\ 0 & f(r) & 0 & 0 \\ 0 & 0 & \frac{1}{r^2} & 0 \\ 0 & 0 & 0 & \frac{1}{r^2 \sin^2 \theta} \end{bmatrix}.$$

Thus,  $A = -B = -C = \frac{3}{L^2}$  and the Ricci scalar is

$$\mathcal{R} = \frac{12}{L^2}. \quad (\text{A5})$$

## 2. RNdS

In this case, the Einstein tensor in a covariant-form is expressed as

$$G^{\mu\nu} = G_{\Lambda}^{\mu\nu} + G_{EM}^{\mu\nu} = -\frac{3}{L^2} \begin{bmatrix} -\frac{1}{f(r)} & 0 & 0 & 0 \\ 0 & f(r) & 0 & 0 \\ 0 & 0 & \frac{1}{r^2} & 0 \\ 0 & 0 & 0 & \frac{1}{r^2 \sin^2 \theta} \end{bmatrix} + \frac{Q^2}{r^4} \begin{bmatrix} \frac{1}{f(r)} & 0 & 0 & 0 \\ 0 & -f(r) & 0 & 0 \\ 0 & 0 & \frac{1}{r^2} & 0 \\ 0 & 0 & 0 & \frac{1}{r^2 \sin^2 \theta} \end{bmatrix}$$

and the remaining relations for  $A$ ,  $B$  and  $C$  are  $A = -B = \frac{3}{L^2} + \frac{Q^2}{r^4}$  and  $C = -\frac{3}{L^2} + \frac{Q^2}{r^4}$ .

In four dimensions the Ricci scalar for the RNdS spacetime has the same value as for the SdS spacetime,

$$\mathcal{R} = \frac{12}{L^2}. \quad (\text{A6})$$

- 
- [1] E. Berti, V. Cardoso and A. O. Starinets, *Class. Quant. Grav.* **26**, 163001 (2009) [arXiv:0905.2975 [gr-qc]].
- [2] K. D. Kokkotas and B. G. Schmidt, *Living Rev. Rel.* **2**, 2 (1999) [gr-qc/9909058].
- [3] H. P. Nollert, *Class. Quant. Grav.* **16**, R159 (1999).
- [4] B. P. Abbott *et al.* [LIGO Scientific and Virgo Collaborations], *Phys. Rev. Lett.* **116**, no. 6, 061102 (2016) doi:10.1103/PhysRevLett.116.061102 [arXiv:1602.03837 [gr-qc]].

- [5] B. P. Abbott *et al.* [LIGO Scientific and Virgo Collaborations], Phys. Rev. Lett. **119**, no. 16, 161101 (2017) doi:10.1103/PhysRevLett.119.161101 [arXiv:1710.05832 [gr-qc]].
- [6] T. Regge and J. A. Wheeler, Phys. Rev. **108**, 1063 (1957). doi:10.1103/PhysRev.108.1063
- [7] A. Nunez and A. O. Starinets, Phys. Rev. D **67**, 124013 (2003) [hep-th/0302026].
- [8] G. T. Horowitz and V. E. Hubeny, Phys. Rev. D **62**, 024027 (2000) [hep-th/9909056].
- [9] S. A. Hartnoll, Class. Quant. Grav. **26**, 224002 (2009) [arXiv:0903.3246 [hep-th]].
- [10] D. T. Son and A. O. Starinets, JHEP **0209**, 042 (2002) [hep-th/0205051].
- [11] K. Lin, J. de Oliveira and E. Abdalla, Phys. Rev. D **90**, no. 12, 124071 (2014) [arXiv:1409.4066 [hep-th]].
- [12] W. Sybesma and S. Vandoren, JHEP **1505**, 021 (2015) [arXiv:1503.07457 [hep-th]].
- [13] E. Abdalla, B. Wang, A. Lima-Santos and W. G. Qiu, “Support of dS / CFT correspondence from perturbations of three-dimensional space-time,” Phys. Lett. B **538**, 435 (2002) [Conf. Proc. C **0208124**, 322 (2002)] [hep-th/0204030].
- [14] E. Abdalla, K. H. C. Castello-Branco and A. Lima-Santos, “Support of dS / CFT correspondence from space-time perturbations,” Phys. Rev. D **66**, 104018 (2002) [hep-th/0208065].
- [15] S. Chandrasekhar, “The Mathematical Theory of Black Holes, 1985, Oxford UK: Clarendon Press, 646 p.
- [16] J. D. Bekenstein, In \*Moscow 1996, 2nd International A.D. Sakharov Conference on physics\* 216-219 [gr-qc/9605059].
- [17] S. S. Gubser, Phys. Rev. D **78**, 065034 (2008) doi:10.1103/PhysRevD.78.065034 [arXiv:0801.2977 [hep-th]].
- [18] M. Rinaldi, Phys. Rev. D **86**, 084048 (2012) doi:10.1103/PhysRevD.86.084048 [arXiv:1208.0103 [gr-qc]].
- [19] M. Minamitsuji, Phys. Rev. D **89**, 064017 (2014) doi:10.1103/PhysRevD.89.064017 [arXiv:1312.3759 [gr-qc]].
- [20] M. S. Volkov and D. V. Gal'tsov, Phys. Rept. **319**, 1 (1999) doi:10.1016/S0370-1573(99)00010-1 [hep-th/9810070].
- [21] S. A. Hartnoll, C. P. Herzog and G. T. Horowitz, JHEP **0812**, 015 (2008) [arXiv:0810.1563 [hep-th]].
- [22] S. A. Hartnoll, C. P. Herzog and G. T. Horowitz, Phys. Rev. Lett. **101**, 031601 (2008) [arXiv:0803.3295 [hep-th]].

- [23] K. Lin, E. Abdalla and A. Wang, *Int. J. Mod. Phys. D* **24**, 0038 (2015) [arXiv:1406.4721 [hep-th]].
- [24] E. Abdalla, J. de Oliveira, A. B. Pavan and C. E. Pellicer, arXiv:1307.1460 [hep-th].
- [25] Q. Pan, B. Wang, E. Papantonopoulos, J. Oliveira and A. B. Pavan, *Phys. Rev. D* **81**, 106007 (2010) [arXiv:0912.2475 [hep-th]].
- [26] E. Abdalla, C. E. Pellicer, J. de Oliveira and A. B. Pavan, *Phys. Rev. D* **82**, 124033 (2010) [arXiv:1010.2806 [hep-th]].
- [27] E. Abdalla, J. de Oliveira, A. Lima-Santos and A. B. Pavan, “Three dimensional Lifshitz black hole and the Korteweg-de Vries equation,” *Phys. Lett. B* **709**, 276 (2012) [arXiv:1108.6283 [hep-th]].
- [28] B. Cuadros-Melgar, J. de Oliveira and C. E. Pellicer, “Stability Analysis and Area Spectrum of 3-Dimensional Lifshitz Black Holes,” *Phys. Rev. D* **85**, 024014 (2012) [arXiv:1110.4856 [hep-th]].
- [29] E. Abdalla, O. P. F. Piedra, F. S. Nuez and J. de Oliveira, “Scalar field propagation in higher dimensional black holes at a Lifshitz point,” *Phys. Rev. D* **88**, no. 6, 064035 (2013) [arXiv:1211.3390 [gr-qc]].
- [30] K. Lin, J. de Oliveira and E. Abdalla, “Holographic phase transition and Quasinormal modes in Lovelock gravity,” *Phys. Rev. D* **90**, no. 12, 124071 (2014) [arXiv:1409.4066 [hep-th]].
- [31] A. Strominger, “The dS / CFT correspondence,” *JHEP* **0110**, 034 (2001) [hep-th/0106113].
- [32] I. L. Buchbinder, S. D. Odintsov and I. L. Shapiro, Bristol, UK: IOP (1992) 413 p
- [33] S. F. Daniel and R. R. Caldwell, Consequences of a Cosmic Scalar with Kinetic Coupling to Curvature, *Class. Quant. Grav.* **24**, 5573 (2007), arXiv:0709.0009.
- [34] C. Gao , When scalar field is kinetically coupled to the Einstein tensor, *JCAP* **023**, 1006 (2010), arXiv:1002.4035.
- [35] S. V. Sushkov, Exact cosmological solutions with nonminimal derivative coupling, *Phs. Rev. D* **80**, 103505, arXiv:0910.0980.
- [36] S. Capozziello, G. Lambiase and H. -J. Schmidt, Nonminimal Derivative Couplings and inflation in Generalized Theories of Gravity, *Annalen Phys.* **9**, 39 (2000), gr-qc/9906051; S. Capozziello, G. Lambiase, Nonminimal Derivative Coupling and the Recovering of Cosmological Constant, *Gen. Rel. Grav.* **31**, 1005 (1999), gr-qc/9901051.
- [37] L. Amendola, Cosmology with non minimal derivative couplings, *Phys. Let. B* **301**, 175 (1993),



gr-qc/9302010.

- [38] S. Chen, Q. Pan and J. Jing, Holographic superconductor models in the non-minimal derivative coupling theory, *Chin. Phys. B* **21**, 040403 (2012), arXiv:1012.3820.
- [39] L. Amendola, M. Litterio and F. Occhionero, *Int. J. Mod. Phys. A* **05**, 3861 (1990).
- [40] R. A. Konoplya and A. Zhidenko, Instability of higher dimensional charged black holes in the de-Sitter world, *Phys. Rev. Lett.* **103**, 161101 (2009), arXiv:0809.2822; R. A. Konoplya and A. Zhidenko, Stability of higher dimensional Reissner-Nordstroem-anti-de Sitter black holes, *Phys. Rev. D* **78**, 104017 (2008), arXiv:0809.2048; R. A. Konoplya and A. Zhidenko, Instability of D-dimensional black holes in Gauss-Bonnet theory, *Phys. Rev. D* **77**, 104004 (2008).
- [41] S. Chen, J. Jing, “Greybody factor for a scalar field coupling to Einstein’s tensor”, *Phys. Lett.* **B691**, 254, (2010);  
S. Chen, J. Jing, “Dynamical evolution of a scalar field coupling to Einstein’s tensor in the Reissner-Nordstroem black hole spacetime”, arXiv:1007.2019, (2010).
- [42] C. Molina, D. Giugno, E. Abdalla, A. Saa, “Field propagation in de Sitter black holes”, *Phys. Rev.* **D69**, 104013, (2004).
- [43] A. Zhidenko, “Quasinormal modes of Schwarzschild de Sitter black holes”, *Class. Quant. Grav.* **21**, 273, (2004).
- [44] R. A. Konoplya, A. Zhidenko, “High overtones of Schwarzschild-de Sitter quasinormal spectrum”, *JHEP* **0406**, 037, (2004);  
R. A. Konoplya, A. Zhidenko, “Instability of higher dimensional charged black holes in the de-Sitter world”, *Phys. Rev. Lett.* **103**, 161101, (2009).
- [45] Da-Ping Du, Bin Wang, Ru-Keng Su, “Quasinormal modes in pure de Sitter space-times”, *Phys. Rev.* **D70**, 064024, (2004).
- [46] G. t Hooft, On the quantum structure of a black hole, *Nucl. Phys. B* **256**, 727 (1985).
- [47] Z. Stuchlk, S. Hledk, “Properties of the Reissner-Nordstroem Spacetimes with a Nonzero Cosmological Constant”, *Acta physica slovacica* **vol. 52 No. 5**.
- [48] R. A. Konoplya, A. Zhidenko, Quasinormal modes of black holes: from astrophysics to string theory, *Rev. Mod. Phys.*, **83**, 793 (2011).
- [49] V. Cardoso and J. O. S. lemos, *Phys. Rev. D* **67**, 084020 (2003), gr-qc/0301078.
- [50] C. Molina, Quasinormal modes of d-dimensional black holes with near extreme cosmological

- constant, Phys. Rev. D **68**, 064007 (2003), gr-qc/0304053.
- [51] P. C. W. Davies, Thermodynamic phase transitions of Kerr-Newman black holes in de Sitter space, Class. Quant. Grav. **6**, 1909 (1989).
- [52] P. r: Brady, C. M. Chambers, W. Krivan and P. Laguna, Telling Tails in the Presence of a Cosmological Constant, Phys. Rev. D **55**, 7538 (1997), gr-qc/9611056.